IJE TRANSACTIONS C: Aspects Vol. 34, No. 03, (March 2021) 587-597

International Journal of Engineering

Journal Homepage: www.ije.ir

Evaluating the Performance of CO Boiler Burners in RFCC Unit using CFD Simulation

A. Aminmahalati[a], A. Fazlali*[a], H. Safikhani[b]

[a] Department of Chemical Engineering, Faculty of Engineering, Arak University, Arak, Iran
[b] Department of Mechanical Engineering, Faculty of Engineering, Arak University, Arak, Iran

PAPER INFO

Paper history:
Received 27 December 2020
Received in revised form 10 January 2021
Accepted 16 January 2021

Keywords:
CFD
Simulation
CO boiler
Mechanisms
Combustion

ABSTRACT

The combustion chamber's internal refractory in Imam Khomeini Oil Refinery Company (IKORC) was damaged in several parts, requiring operating conditions and re-inspecting the design of the combustion chamber using CFD. Simplify the combustion chamber 3D simulation, decrease in the number of calculations, the symmetry principle was applied in the simulation. The results, independent of the mesh network, were investigated via increasing the mesh nodes. The one-stage, two-stage, multi-stage and overall mechanisms, which were designated, were examined and compared to actual measured data and a calculation error of less than 8% was obtained. Ultimately, selecting overall mechanisms, the simulation results, streams mixing and length of the chamber were scrutinized, and as a result, the current design was approved. The temperature and velocity of the flows in the combustion chamber were investigated. In the combustion chamber, the farther we are from the burners, the more uniform the velocity and temperature profiles also become as the wall temperature increases. The rate of combustion reaction was evaluated with the temperature of different points in the combustion chamber. The results showed that the combustion chamber wall's temperature is in the appropriate range and has not suffered any thermal damage. Unlike the combustion chamber wall, the burner wall (at the mixing point) has an unauthorized temperature; there is the possibility of thermal damage that can be eliminated by changing the number of currents. Unsuitable thermal profiles also showed large amounts of oxygen in the exhaust gas indicated that the steam boiler performance is far from the optimal condition and specific changes would be required in the air streams. Streamline demonstrated that the primary air stream was more effective for decreasing CO and NO_X amounts in the outlet stream. The secondary air stream was also significant to prevent thermal damage to the internal coating and reduce safety hazards.

doi: *10.5829/ije.2021.34.03c.01*

1. INTRODUCTION

The increasing rate of fossil fuel consumption, such as coal, crude oil and natural gas, followed by a gradual reduction in their reservoirs, has become one of the most controversial contemporary issues. Exhausting fossil fuels harm the environment and cause significant environmental damages. Their consumption leads to CO_2 and CO production, and consequently, a continuous increase in greenhouse gas emissions. Despite the highly damaging impacts of CO_2 on global warming, the effects of CO are negligible. Nevertheless, it is noteworthy to mention that CO has significant indirect impacts. It reacts with the OH-radicals in the atmosphere, which behaves as an inhibitor for greenhouse gases, such as methane. Also, CO can boost the formation of Ozone [1]. Therefore, more improvement is vital in combustion technologies and processes [2].

There are several different codes for numerical calculations. These codes can generally be classified into LP codes and Computational Fluid Dynamics (CFD) codes. The significant advantage of CFD codes is their capability to model the turbulent flows and complex geometries. However, the most significant impediment of this class is their high computational costs. On the other hand, LP codes are suited to handle merely simple

Corresponding Author Institutional Email: a-fazlzli@araku.ac.ir (A. Fazlali)

Please cite this article as: A. Aminmahalati, A. Fazlali, H. Safikhani, Investigating the Performance of CO Boiler Burners in the RFCC Unit with CFD Simulation, International Journal of Engineering, Transactions C: Aspects Vol. 34, No. 03, (2021) 587-597

geometries and their biggest strength lies in their capability of running the equation fast [3]. For example, CFD codes and other simulation methods have been used to research references [4-11]. In CFD, we attempt to model combustion utilizing simple reaction models because detailed chemical reaction mechanisms are composed of hundreds of species and side reactions that cannot accommodate reasonable costs. Moreover, an increase in the number of different reaction mechanisms adds to the overall modeling complexity [2].

According to the inherent intricacy of interaction among turbulency, combustion, convection, radiation, buoyancy and compressibility of gases, CFD combustion modeling is a complex subject. This complexity rises specifically in large chambers when natural, or forced convection must be considered. Thus, CFD combustion modeling requires being validate using physical and empirical results. Validation of CFD codes promotes certainty of users in its forecast precision. Modeling validation is of significance regarding complicated cases. However, validation tests are not applicable since they are costly and challenging to be implemented [12]. CFD focus and strength have been on predicting reaction structure, temperature, velocity and not the emission of pollutants [2].

In the oil refinery's RFCC units, a 700-800°C gaseous phase flows out of the regeneration unit. It carries less than 5% of CO and the rest includes N_2, H_2O and CO_2, which is called flue gas [12].

CO burns with fuel gas in CO boilers, generating a vast amount of heat. Hot gases from combustion are then cooled down via heat exchangers using cooling water in tubes. This interaction leads to superheated steam production and the utility units can apply the steam. Refineries deal with significant daily steam demands. Accordingly, the CO boiler steam production can mainly cut the costs down. Since then, CO boilers play a pivotal role in the RFCC process [12].

The CO boiler internal wall is installed to protect the refractory from thermal damages. The CO boiler temperature can rise to 1200°C. Furthermore, this may cause internal/external damages; for instance, high temperatures can damage central refractories [12].

A typical CO boiler generates up to 300 tons of steam per hour. This production annually reduces the expenses in the refinery by 68 million dollars [13]. The CO boiler maintenance, inspection and shut down have substantial consequences in the RFCC process and any damage would lead to a loss of 1 million dollars per day. Also, possible threats to human and environmental safety are crucial when the CO boiler is shut down [12-14]

The present study was conducted to investigate the combustion chamber performance and its effects on the refractory's internal wall. The above-mentioned CO boiler produces 270 tons of high-pressure steam an hour, RFCC unit in Imam Khomeini Oil Refinery Company (IKORC). Two combustible streams of fuel gas and flue gas flow into the chamber. Fuel gas stream is composed of butane and lighter gases. Table 1 represents the property details of this stream .The flue gas stream is the regeneration unit output and it contains 1.25% of carbon monoxide and a small amount of oxygen and other non-combustible compounds. The required oxygen is supplied with two air streams. The required oxygen is supplied with two air streams (primary and secondary air). Table 1 contains all the mentioned streams in detail. The flue gas stream has a high temperature (702°C) and the other three streams (fuel gas, primary and secondary air) enter the combustion chamber at a temperature close to the environment. The output streamline from the combustion chamber enters the steam generator heat exchanger and its temperature is important in the amount of steam production [15].

Once the CO boiler is not in service, in addition to the enormous energy loss, a considerable amount of CO is released into the environment. Therefore, timely diagnosis and proper maintenance of internal walls in the CO boiler will decrease possible maintenance and prevent environmental pollution. The flowchart used for this research is shown in Figure 1.

Significant damages have been spotted in the refractory cover of the walls. In case of a lack of diagnosis regarding the damages, financial losses are expected, and wall raptures may lead to operators' casualties. In this work, the chamber's flame profile was investigated and the reason for the current damages was represented. This study focuses specifically on the flame in the combustion chamber and examines its effects in the combustion chamber, especially its walls exhaust gas compositions and It also investigates the effect of flame on combustion gas compositions. In other words,

TABLE 1. Properties and components of the chamber inlet streamlines

		Unit	Flue gas	Fuel gas	Primary Air	Secondary air
Flow		$kg/_s$	34.2	0.41	6.5	6.5
Temperature		C	702	60	50	50
Compounds of constituent	**H_2**	%	-	13.6	-	-
	CH_4	%	-	65.22	-	-
	C_2H_6	%	-	5.16	-	-
	C_3H_8	%	-	3.24	-	-
	$C_4H_{10}^+$	%	-	1.86	-	-
	CO	%	1.25	-	-	-
	CO_2	%	17.22	0.33	-	-
	N_2	%	80.3	10.59	79.81	79.81
	O_2	%	0.13	-	20.19	20.19

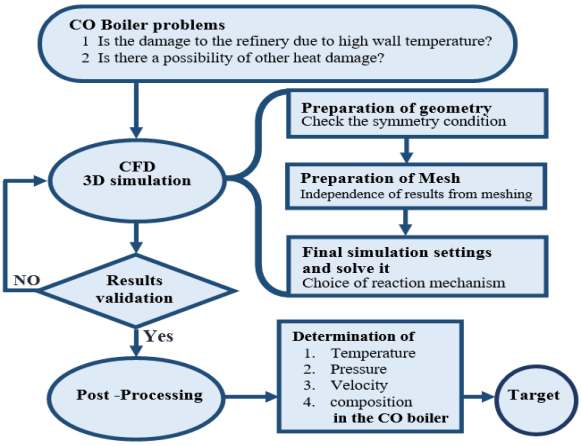

Figure 1. Flowchart of the methodology used in the present work

this study seeks to understand better the effects of flame in the combustion chamber and ways to improve the economic and environmental performance of the CO boiler.

2. BURNER MODELING

2. 1. Physical Model As illustrated in Figure 2, the combustion chamber is a 900 m^3 cylinder with three identical burners, in which three similar sets of burners are installed. Each group consists of 9 smaller burners, one in the center and the rest are located in the chamber circumference.

Due to the large volume of the chamber, a numerous mesh network is required. The symmetrical principles are significantly applied to cut down the simulation model volume. As shown in Figure 3, splitting the chamber into three subdivisions, streams in each burner set are not

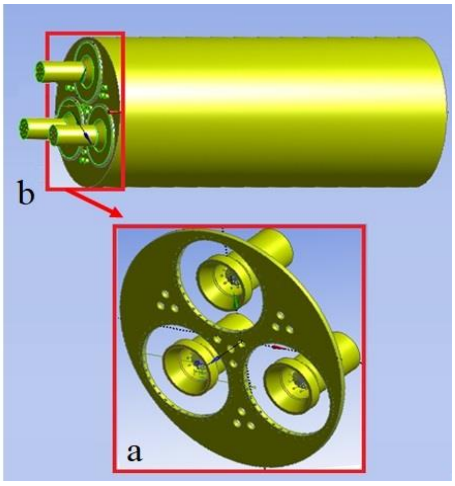

Figure 2. Stimated boiler combustion chamber a) Overall view b) Burners zone

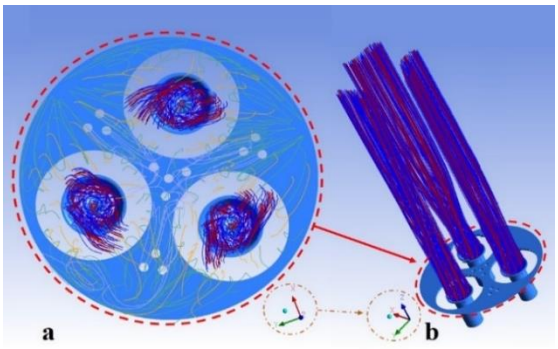

Figure 3. Co boiler streamlines. a) Streamlines overall view b) Fuel gas and primary air streamlines

intermixed. The smaller volume, there is to model, the denser the mesh network we will get. Figure 3 illustrates all the streamlines of the steam boiler. Figure 3.a indicates streamlines and symmetrical principle effects, and Figure 3.b represents the primary air and the fuel gas streams. According to Figure 3, it can be concluded that no stream intermix occurs.

Figure 4 shows all the entering streams to the chamber. Figure 4.a represents the combustion chamber, and Figure 4.b demonstrates the inlet section of the chamber. Flue gas is sprayed from the periphery of the torch, shown as α in yellow. The primary air streams inflow the burners from internal rings, while the external rings and holes located at the outer ring circumference supply the secondary air. Due to the symmetry of the combustion chamber, one-third of the combustion chamber is modeled. The secondary air is divided into two parts; part one is in the form of external rings around flue gas, depicted as the thin rings as shown β in blue in

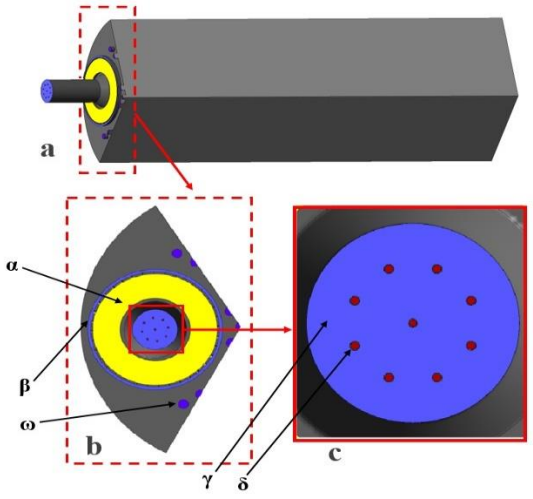

Figure 4. Simulated chamber inlet streamlines **a)** Overall view of the combustion chamber, **b)** magnified view of the inlets and **c)** magnified view of the inlets to the burner α-Inlet Flue gas, **β**-Internal ring: primary air inlet, **ω**-External ring and holes: secondary air inlets, **γ**-Primary air, **δ**-Inlet fuel gas

Figure 4.b. The part two ,consists of small circles shown as ω in blue. The primary air stream is illustrated in Figures 4.b and 4.c. It is shown to be charged to the burner center represented as γ in blue. The input venue for fuel gas includes nine small circles represented in Figure 4.c as δ in red.

As illustrated in Figure 5, the wall temperature was of the maximum error. When we do calculations with 3 million, this error progressively decreased to 1%. Other variable deviation errors in this node number were less than 0.3%. With the increase in mesh nodes up to 6 million, all the errors decreased to below 0.1%. Table 2 shows important information about meshing, including simulation volume, the maximum and minimum size of each mesh, the growth rate of mesh size, number of nodes and number of elements.

2. 2. Numerical Method The ANSYS/CFX v19.0 software was used for CFD simulations by solving the numerical simulation carried out on a supercomputer with Intel Xeon CPU E5-2630L V2(2.4 GHz * 8 CPUs, 30 GB RAM). The mathematical modeling in this study is based on a steady-state condition. The turbulence equation is standard k–ε [16-18]. The buoyancy force was neglected in the gas type and steam boiler horizontal geometry, following the simulation results. Three different heat transfer governing equations are optionally available. Meanwhile, due to combustion reaction nature and high fluid temperature variations, the overall energy governing equation was designated.

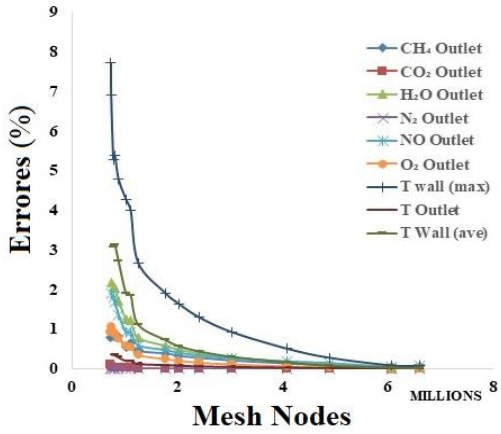

Figure 5. Mesh network independency deviation (major variables deviation) vs. nodes number

TABLE 2. Important information about meshing, which is: simulation volume, the maximum and minimum size of each mesh, the growth rate of mesh size, number of nodes and number of elements

Volume (m^3)	Max face size (mm)	Min size (mm)	Growth rate	NO. nodes	NO. elements
290.68	25	1	1.2	6.17e+6	3.45e+7

Typical and defined reactions in the simulation must cover combustions of methane, butane, ethane, propane, CO and H_2. Accordingly, the three mechanisms are suggested as follows: One-stage, two-stage and multi-stage reaction mechanism. Westbrook and Dryer [34] proposed several simplified reaction mechanisms for the oxidation of fuels, namely the WD one-step (WD1), WD two-step (WD2) and multi-step with Water-Gas Shift reaction (WGS) mechanisms. Table 3 shows the different mechanisms used for the combustion reaction in the CO boiler. All the three mechanisms, as mentioned earlier, were applied in different simulations separately; meanwhile, the fourth simulation was applied with all the mechanisms simultaneously. A brief literature review is presented in Table 4 concerning the combustion reactions in the three mechanisms.

Generally, thermal radiation with different models was studied and here, model P1 is considered [35-37]. P1 is a simple and accurate model and suitable for simulating large objects.

3. MODEL VALIDATION

Validation was confirmed by adapting actual and empirical temperature and analysis of steam boiler exhaust gases with results calculated by the simulation. Four thermometers were set up on the steam boiler. The control system gathered the mean temperature data as one of the significant parameters to control the combustion chamber. Actual and calculated temperatures are listed in Table 5. The thermometers were installed in one direction with the same distance to burners. Figure 6 illustrates the direction of the thermometer. Figure 7 simulates the thermometer's changes in the thermometer's direction. The simulation shows that it can be observed that the maximum temperature difference in the thermocouple direction was 21°C. If an accurate thermometers show more difference, they are damaged. The simulation shows that The difference between the average of the wall temperatures and the average temperature of the exhaust gas was less than 8°C. Therefore, the average of the wall temperatures is a desirable criterion for estimating the outlet temperature.

Table 5 represents the compared values for the exhaust gas analysis and four simulated reaction mechanisms. The experimental values were dry-based. The listed result in Table 5 indicates that the overall reaction mechanism results are closer to the real data. Defining the error function below (Equation (1)), the simulation's temperature error for combining mechanisms was less than 6%; however, each mechanism's deviation was estimated to be less than 7%.

$$Erorr = \frac{(Real\ Data - Simulation\ data)}{Real\ Data} \quad (1)$$

TABLE 3. Single-stage, two-stage and multi-stage reaction mechanisms in CO boiler

	One-stage reactions (WD1)	Two-stage reactions (WD2)	Multi-stage reactions (WGS)
Butane	$C_4H_{10} + 6.5O_2 \xrightarrow{k[O_2]^{1.6}[C_4H_{10}]^{0.15}} 4CO_2 + 5H_2O$	$C_4H_{10} + 4.5O_2 \xrightarrow{k[O_2]^{1.6}[C_4H_{10}]^{0.15}} 4CO + 5H_2O$ $CO + 0.5O_2 \xrightarrow[H_2O]{k[CO][H_2O]^{0.5}[O_2]^{0.25}} CO_2$	$C_4H_{10} + 2O_2 \xrightarrow{k[O_2]^{1.6}[C_4H_{10}]^{0.15}} 4CO + 5H_2$ $CO + 0.5O_2 \xrightarrow[H_2O]{k[CO][H_2O]^{0.5}[O_2]^{0.25}} CO_2$ $H_2 + 0.5O_2 \longrightarrow H_2O$ $CO + H_2O \longleftrightarrow CO_2 + H_2$
Propane	$C_3H_8 + 5O_2 \xrightarrow{k[O_2]^{1.65}[C_3H_8]^{0.1}} 3CO_2 + 4H_2O$	$C_3H_8 + 3.5O_2 \xrightarrow{k[O_2]^{1.65}[C_3H_8]^{0.1}} 3CO + 4H_2O$ $CO + 0.5O_2 \xrightarrow[H_2O]{k[CO][H_2O]^{0.5}[O_2]^{0.25}} CO_2$	$C_3H_8 + 1.5O_2 \xrightarrow{k[O_2]^{1.65}[C_3H_8]^{0.1}} 3CO + 4H_2$ $CO + 0.5O_2 \xrightarrow[H_2O]{k[CO][H_2O]^{0.5}[O_2]^{0.25}} CO_2$ $H_2 + 0.5O_2 \longrightarrow H_2O$ $CO + H_2O \longleftrightarrow CO_2 + H_2$
Ethane	$C_2H_6 + 3.5O_2 \xrightarrow{k[O_2]^{1.65}[C_2H_6]^{0.1}} 2CO_2 + 3H_2O$	$C_2H_6 + 2.5O_2 \xrightarrow{k[O_2]^{1.65}[C_2H_6]^{0.1}} 2CO_2 + 3H_2O$ $CO + 0.5O_2 \xrightarrow[H_2O]{k[CO][H_2O]^{0.5}[O_2]^{0.25}} CO_2$	$C_2H_6 + O_2 \xrightarrow{k[O_2]^{1.65}[C_2H_6]^{0.1}} 2CO + 3H_2$ $CO + 0.5O_2 \xrightarrow[H_2O]{k[CO][H_2O]^{0.5}[O_2]^{0.25}} CO_2$ $H_2 + 0.5O_2 \longrightarrow H_2O$ $CO + H_2O \longleftrightarrow CO_2 + H_2$
Methane	$CH_4 + 2O_2 \xrightarrow{k\frac{[O_2]^{1.3}}{[CH_4]^{0.3}}} CO_2 + 2H_2O$ $0.5N_2 + 0.5O_2 \xrightarrow[CH_4]{k[N_2][CH_4][O_2]^{0.5}} NO$ $N_2 + O_2 \xrightarrow{k[N_2][O_2]^{0.5}} 2NO$	$CH_4 + 1.5O_2 \xrightarrow{k\frac{[O_2]^{1.3}}{[CH_4]^{0.3}}} CO + 2H_2O$ $CO + 0.5O_2 \xrightarrow[H_2O]{k[CO][H_2O]^{0.5}[O_2]^{0.25}} CO_2$ $0.5N_2 + 0.5O_2 \xrightarrow[CH_4]{k[N_2][CH_4][O_2]^{0.5}} NO$ $N_2 + O_2 \xrightarrow{k[N_2][O_2]^{0.5}} 2NO$	$CH_4 + 0.5O_2 \xrightarrow{k\frac{[O_2]^{1.3}}{[CH_4]^{0.3}}} CO + 2H_2$ $CO + 0.5O_2 \xrightarrow[H_2O]{k[CO][H_2O]^{0.5}[O_2]^{0.25}} CO_2$ $H_2 + 0.5O_2 \longrightarrow H_2O$ $CO + H_2O \longleftrightarrow CO_2 + H_2$ $0.5N_2 + 0.5O_2 \xrightarrow[CH_4]{k[N_2][CH_4][O_2]^{0.5}} NO$ $N_2 + O_2 \xrightarrow{k[N_2][O_2]^{0.5}} 2NO$
Monoxide Carbone	$CO + 0.5O_2 \xrightarrow[H_2O]{k[CO][H_2O]^{0.5}[O_2]^{0.25}} CO_2$	$CO + 0.5O_2 \xrightarrow[H_2O]{k[CO][H_2O]^{0.5}[O_2]^{0.25}} CO_2$	$CO + 0.5O_2 \xrightarrow[H_2O]{k[CO][H_2O]^{0.5}[O_2]^{0.25}} CO_2$
Hydrogen	$H_2 + 0.5O_2 \longrightarrow H_2O$	$H_2 + 0.5O_2 \longrightarrow H_2O$	$H_2 + 0.5O_2 \longrightarrow H_2O$

TABLE 4. Brief literature review

NO.	The subject under study	Power (MW)	WD1	WD2	WGS	Ref.
1	circulating fluidized bed (CFB) boiler	660	√			[19]
2	circulating fluidized bed (CFB) boiler	350	√			[20]
3	ultra-supercritical BP 680 boiler	200		√		[21]
4	pulverized coal boilers	160		√	√	[22]
5	biomass boilers	35		√		[23]
6	circulating fluidized bed (CFB) boiler	12	√			[24]
7	reciprocating grate boiler	4		√		[25]
8	oxy-fuel combustion with pulverized coal	2.5			√	[26]
9	biomass combustion	0.3			√	[27]
10	MILD combustion furnace	0.02		√	√	[28]
11	residential furnace	0.015			√	[29]
12	Moderate or intense low-oxygen dilution (MILD) combustion	.0130			√	[30]
13	combustion in a bubbling fluidized bed	-	√	√	√	[31]
14	Flameless Combustion	-		√		[2]
15	swirled burner combustion	-		√		[32]
16	industrial low swirl burner combustion	-		√		[1]
17	rocket combustor	-		√		[33]
18	explosions in straight large-scale tunnels	-	√			[17]

TABLE 5. Compared values for exhaust gas and simulated exhaust gas

Compounds	T	O_2	CO_2	CO
Units	^{O}C	%	%	ppm
WD1	806.94	6.32	18.412	1

WD2	807.80	6.33	18.388	2.3
WDG	807.75	6.32	18.39	2.9
Combined Mechanisms	799.23	6.32	18.386	0.6
Real results	757	6.6	17.8	4

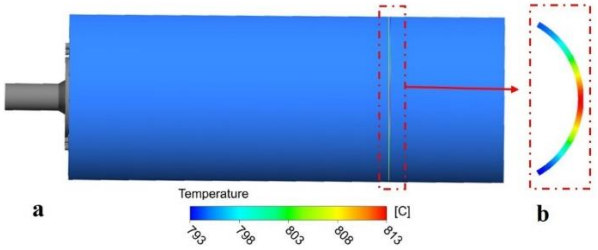

Figure 6. Thermometers' direction in the chamber. a) Overall view and thermometers direction location and b) temperature profile in the direction in the chamber

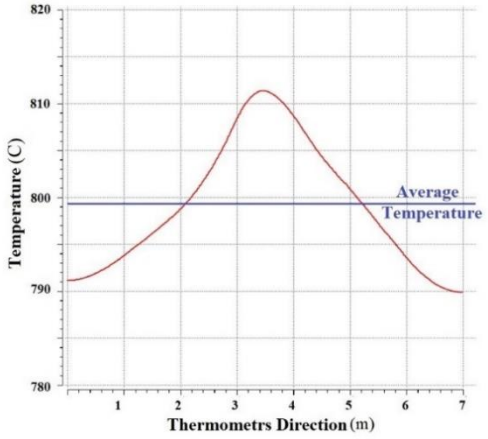

Figure 7. The temperature changes thermometers direction and averages them

Reporting stream flow in the chamber shows that the error rate of 5% is acceptable for industrial flow meters. We attempted to reduce this error by accurate calibration. This error was under 8% for CO_2 and O_2 and since the CO amount was negligible, the error function would not be a suitable option.

4. RESULTS AND DISCUSSIONS

Different streams flow in different combustion chamber sectors, which causes the flow profile to form in the combustion chamber. Combustion causes the temperature change, resulting in an amendment in the gases' velocity inside the combustion chamber. Figure 8 represents the velocity changes in the chamber, which is composed of three parts. In the upper and lower parts, the velocity profile is shown in the cross-section, while the middle part of the figure indicates the middle section of the chamber. Additionally, each of the cross-sections is pointed out in the middle section. Figure 8 indicates that the maximum velocity was observed in burner exhausts and that the closer we got to the end of the chamber, the more uniform flow we had.

Figure 9 illustrates the wall temperature for all four mechanisms. As can be seen, the three mechanisms' general profiles were almost the same, yet it was different for the overall mechanism profile. Moreover, the reaction temperature increased as we got closer to the end of the chamber.

Temperature changes in the combustion chamber's flames can be seen through its few cross-sections in Figure 10. Figure 10 shows that firstly, the heat accumulated in the center, and then, by moving away

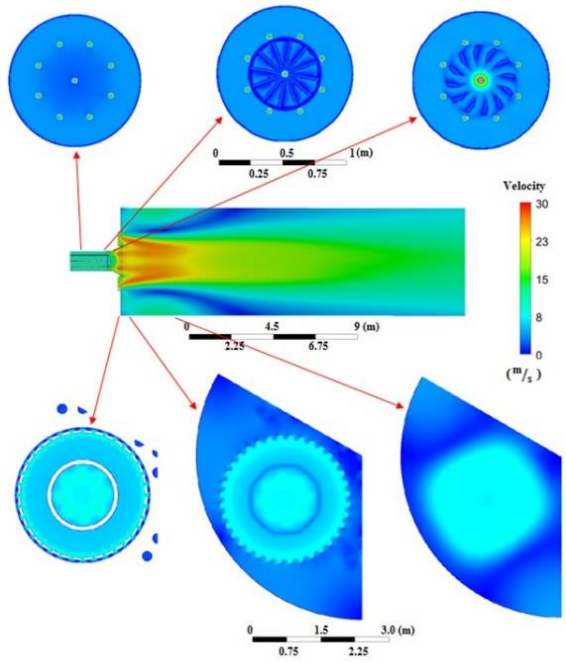

Figure 8. The velocity profiles in different cross-sections in the chamber

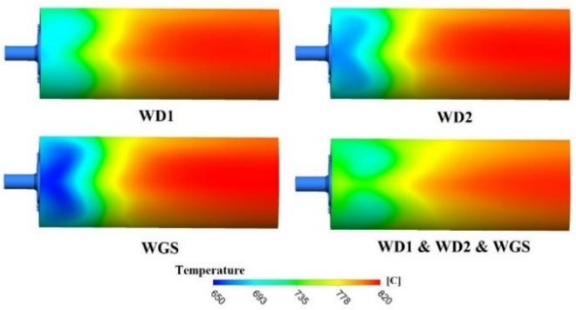

Figure 9. The chamber walls temperature profiles in different mechanisms

from the burners, the intermixing of flows reduces the temperature difference. As it can be seen in Figure 10, the burner's wall temperature increased and our calculations revealed that this temperature could reach to 1017°C. While the vendor's maximum allowable temperature in refractory is announced to be less than 982°C. This increase of 35°C indicates the possible occurrence of the damage.

Two parallel cross-sections adjoining burners are shown in Figure 11, representing flames profile changes as cold air was added to the flow. In Figure 11.a, mixing air and fuel gas is illustrated where combustion occurred around the central burner. According to Figure 11.b, the flame profile was fully developed due to air and fuel gas combustion. As shown in Figure 11, with an increase in the airflow, refractory would cool down; therefore, the temperature rising issue detected in Figure 10 was solved.

In Figure 12, we increased the burner's distance so that flame profiles would be in three cross-sections in 0.5, 5 and 15 m distance from the burner. As it can be seen in Figure 12.a, the temperature difference was higher than 1800°C while whereas this difference reduced significantly to less than 52°C according to Figure 12.c.

According to Figures.10-12, it can be concluded that in the combustion chamber, as we got approached to the end of the chamber, the temperature difference between fluid and wall decreased. In the center of the burner, the flame's core was at high temperature and the end of the chamber, no significant difference was detected. These results reveal that walls at the end of the chamber are more vulnerable to possible temperature rising damages.

Figure 13 illustrates a 3D image of the flame profile in the combustion chamber. Detecting the temperatures above a specified value, the profiles were obtained. Herein, the specified values were the temperatures above 1200, 982 and 850°C, respectively. At temperatures above 1200°C, we only had a profile in front of the burner. At lower temperatures, the profiles were developed. A remarkable issue represented in Figure 13 is that the flame, profiles even at 850°C, is not close adequately to any walls of the chamber and the flame was

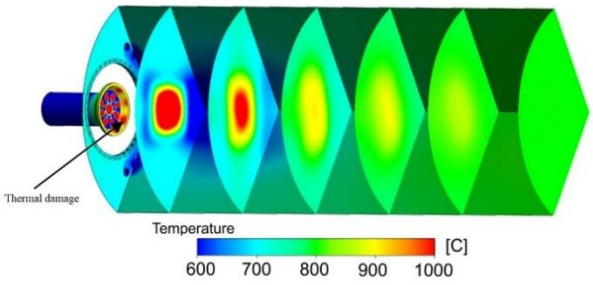

Figure 10. The flame temperature changes in different cross-sections of the chamber

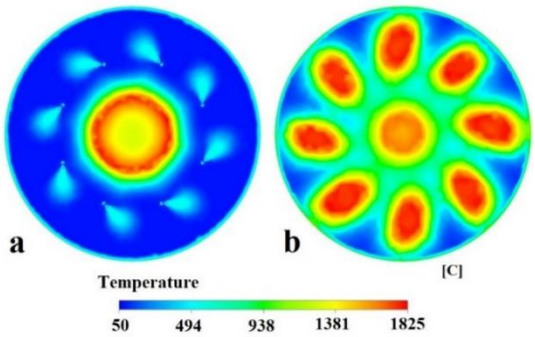

Figure 11. The temperature profile in two different sections near the burner

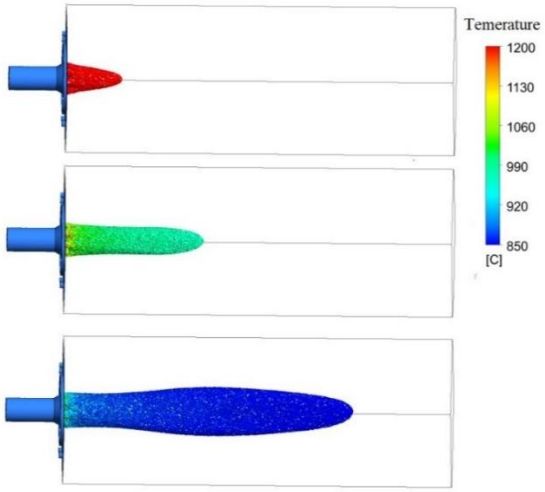

Figure 13. Flame profile 3D image

centrally developed. As mentioned before, 982°C is the maximum allowable temperature for the walls, indicating that construction problems might trigger refractory damage in sidewalls.

As mentioned, four streams enter the simulation combustion chamber, including primary air, secondary air, fuel gas and flue gas. The secondary air entered the chamber in two different spots, which can be seen in Figure 4c. The streamlines are illustrated in Figs.14 and 15. The streamline shows the path through which each stream flowed in the chamber. Figure 14 represents primary air, secondary air and their mixture streams. Figure 15 illustrates a combination of streams in which the primary air stream covered fuel gas and supplied the combustion that required oxygen. In the case of excess air, this amount of air helps obtain the full combustion of CO. Figure 15.a shows the mixture of air and fuel gas. As shown in Figure 15.b, the secondary air streams surrounded CO content flows and initially supplied this reaction, which required oxygen. In the case of excessive air, it helps fuel gas combustion. Figure 15.c illustrates all the flow mixtures.

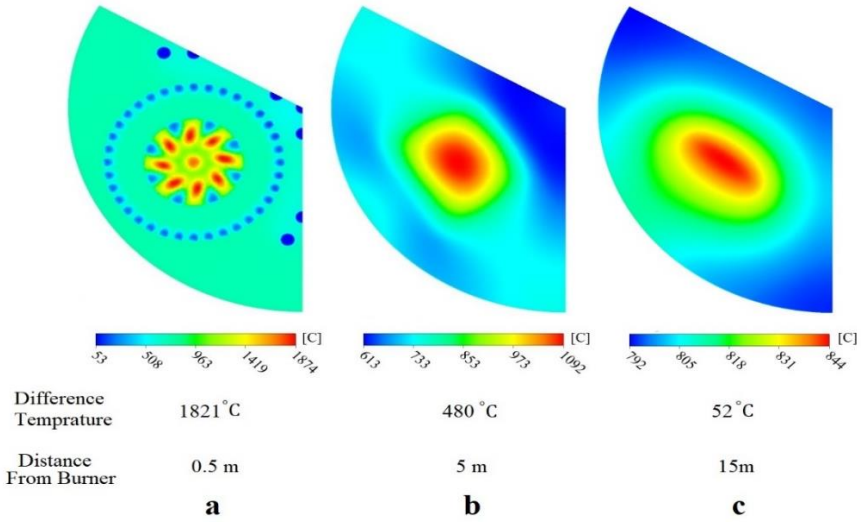

Figure 12. Temperature profile at cross-sections in different distances from the burner

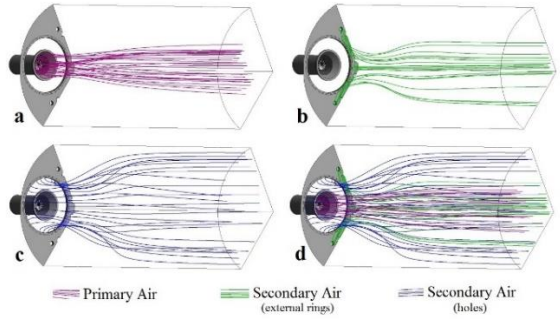

Figure 14. Inlet air streamlines. a) Primary air, b) secondary air (external ring), c) Secondary air (holes) and d) Total inlet air streamlines

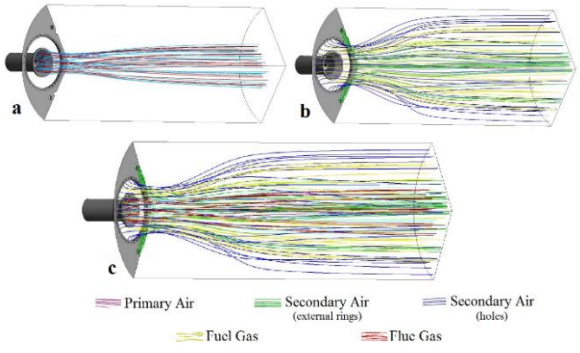

Figure 15. Inlet air streamlines. a) Primary air and fuel gas, b) Secondary air and flue gas and c) Total inlet streamlines

Figure 16 illustrates the reaction progress as a result of the reduction in reactants in the streamlines. This figure shows that molar fractions of CH_4, C_2H_6, C_3H_8 and C_4H_{10} rapidly reduced, which led to a decrease in the reaction rate. Meanwhile, the CO reaction rate was far slower compared to the other components. Furthermore, according to the temperature differences of various streamlines and high CO combustion dependency on temperature, CO velocity differed from the other reactants. Figure 17 illustrates the Oxygen rate changes in the primary and secondary air streams. As could be perceived, the primary air reacted faster than the secondary one. The difference between primary and secondary air reaction rates is due to the different mixing of them with other streams.

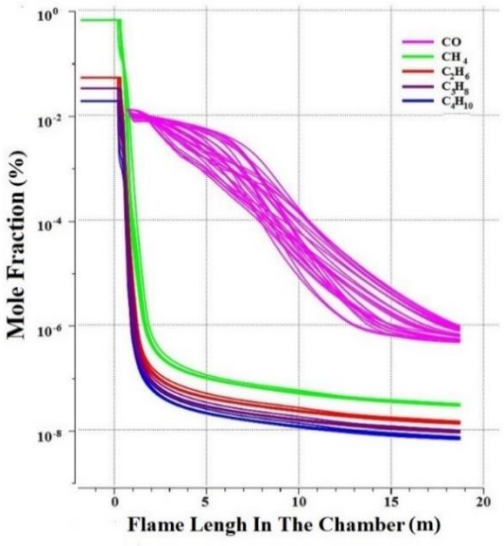

Figure 16. Reaction progress in the chamber via reactions changes

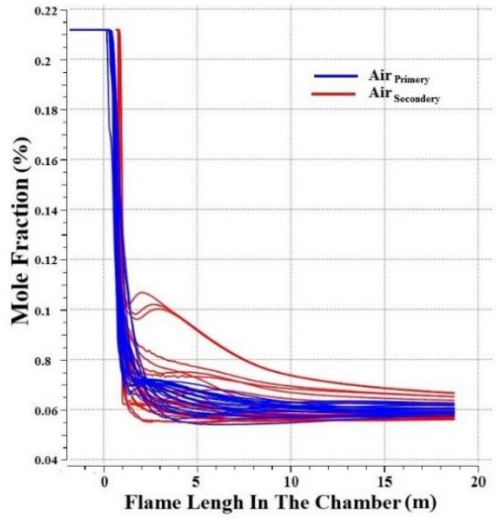

Figure 17. Oxygen level change in primary and secondary air streamlines

5. CONCLUSION

The combustion chamber of the CO boiler corresponding to the RFCC unit of the IKORC was simulated. Streamlines showed that the conditions of symmetry in the combustion chamber could be used. Also, the condition of non-dependence of the simulation results on the mesh size was investigated. The simulation results for one-stage, two-stage, multi-stage and overall combustion mechanisms showed that the closest simulation result to the actual results is the overall mechanisms. Comparison of real and simulation results shows that the simplification assumptions and calculations performed have a total error of less than 8%.

Flame velocity and temperature profiles were plotted. The results show that the flames are in the center of the combustion chamber and do not damage the combustion chamber wall, but as shown in Figure 9, there is a possibility of damage to the burner wall.

According to Figures 16 and 8, the combination of streams in the chamber was well-designed. Figure 16 also shows that the CO fraction slope decreased at the end of the chamber to reach less than 1%; thus, the chamber's length was optimally designed. Regarding Figures.14 and 15, the following results can be derived:

1. Primary air was applied for fuel gas combustion. Since then, any change in this factor altered the primarily required air.
2. Secondary air was applied for CO content stream combustion. Since then, any change in this factor alters the air required as secondary.
3. Primary air was more effective in the center, while the secondary air affects the walls. Therefore, to regulate wall temperatures, the secondary air needed to be changed. On the other hand, any other changes in CO and NO content streams require alteration of the primary air.

The maximum allowable temperature in the refractory was not observed in the burner, yet the wall temperature was much less than the allowable temperature. It can be concluded that refractory damage is not associated with functional temperature .

To prevent further damage to the burner, it is recommended to increase the primary air or modify it. Concerning the wall temperature, it is suggested to reduce the secondary air to increase thermal efficiency. The optimal amount of oxygen for burners was calculated to be approximately 3; accordingly, it is recommended to reduce the chamber's overall air entrance .This modification increases thermal efficiency and decreases fuel consumption, which ultimately reduces environmental pollution.

6. REFERENCES

1. Cellek, M.S. and Pınarbaşı, A., "Investigations on performance and emission characteristics of an industrial low swirl burner while burning natural gas, methane, hydrogen-enriched natural gas and hydrogen as fuels", ***International Journal of Hydrogen Energy***, Vol. 43, No. 2, (2018), 1194-1207, DOI: 10.1016/j.ijhydene.2017.05.107.
2. Perpignan, A.A.V., Sampat, R. and Gangoli Rao, A., "Modeling pollutant emissions of flameless combustion with a joint cfd and chemical reactor network approach", ***Frontiers in Mechanical Engineering***, Vol. 5, (2019), DOI: 10.3389/fmech.2019.00063.
3. Cherbański, R. and Molga, E., "Cfd simulations of hydrogen deflagration in slow and fast combustion regime", ***Combustion Theory and Modelling***, Vol. 24, No. 4, (2020), 589-605, DOI: 10.1080/13647830.2020.1724336.
4. Aminoroayaie Yamini, O., Mousavi, S.H., Kavianpour, M.R. and Movahedi, A., "Numerical modeling of sediment scouring phenomenon around the offshore wind turbine pile in marine environment", ***Environmental Earth Sciences***, Vol. 77, No. 23, (2018), DOI: 10.1007/s12665-018-7967-4.
5. Sengupta, A.R., Gupta, R. and Biswas, A., "Computational fluid dynamics analysis of stove systems for cooking and drying of muga silk", ***Emerging Science Journal***, Vol. 3, No. 5, (2019), 285-292, DOI: 10.28991/esj-2019-01191.
6. Dirbude, S.B. and Maurya, V.K., "Effect of uniform magnetic field on melting at various rayleigh numbers", ***Emerging Science Journal***, Vol. 3, No. 4, (2019), 263-273, DOI: 10.28991/esj-2019-01189.
7. Movahedi, A., Kavianpour, M.R. and Aminoroayaie Yamini, O., "Evaluation and modeling scouring and sedimentation around downstream of large dams", ***Environmental Earth Sciences***, Vol. 77, No. 8, (2018), DOI: 10.1007/s12665-018-7487-2.
8. Movahedi, A., Kavianpour, M. and Aminoroayaie Yamini, O., "Experimental and numerical analysis of the scour profile downstream of flip bucket with change in bed material size", ***ISH Journal of Hydraulic Engineering***, Vol. 25, No. 2, (2017), 188-202, DOI: 10.1080/09715010.2017.1398111.
9. Gharibshahian, E., "The effect of polyvinyl alcohol concentration on the growth kinetics of ktiopo4 nanoparticles synthesized by the co-precipitation method", ***HighTech and Innovation Journal***, Vol. 1, No. 4, (2020), 187-193, DOI: 10.28991/hij-2020-01-04-06.
10. Jabbarzadeh Sani, M., "Spin-orbit coupling effect on the electrophilicity index, chemical potential, hardness and softness of neutral gold clusters: A relativistic ab-initio study", ***HighTech***

and Innovation Journal, Vol. 2, No. 1, (2021), 38-50, DOI: 10.28991/hij-2021-02-01-05.

11. Trang, G.T.T., Linh, N.H., Linh, N.T.T. and Kien, P.H., "The study of dynamics heterogeneity in SiO_2 liquid", ***HighTech and Innovation Journal***, Vol. 1, No. 1, (2020), 1-7, DOI: 10.28991/hij-2020-01-01-01.
12. Yeh, C.-L., "Numerical analysis of the combustion and fluid flow in a carbon monoxide boiler", ***International Journal of Heat and Mass Transfer***, Vol. 59, (2013), 172-190, DOI: 10.1016/j.ijheatmasstransfer.2012.12.020.
13. Yeh, C.-L., "Numerical investigation of the heat transfer and fluid flow in a carbon monoxide boiler", ***International Journal of Heat and Mass Transfer***, Vol. 55, No. 13-14, (2012), 3601-3617, DOI: 10.1016/j.ijheatmasstransfer.2012.02.073.
14. Yeh, C.L. and Liang, C.W., "Nox reduction in a carbon monoxide boiler by reburning", ***Procedia Engineering***, Vol. 67, (2013), 378-387, DOI: 10.1016/j.proeng.2013.12.037.
15. Aminmahalati, A., Fazlali, A. and Safikhani, H., "Multi-objective optimization of CO boiler combustion chamber in the RFCC unit using NSGA II algorithm", ***Energy***, Vol. 221, (2021), DOI: 10.1016/j.energy.2021.119859.
16. Echi, S., Bouabidi, A., Driss, Z. and Abid, M.S., "Cfd simulation and optimization of industrial boiler", ***Energy***, Vol. 169, (2019), 105-114, DOI: 10.1016/j.energy.2018.12.006.
17. Zhu, Y., Wang, D., Shao, Z., Zhu, X., Xu, C. and Zhang, Y., "Investigation on the overpressure of methane-air mixture gas explosions in straight large-scale tunnels", ***Process Safety and Environmental Protection***, Vol. 135, (2020), 101-112, DOI: 10.1016/j.psep.2019.12.022.
18. Jóźwiak, P., Hercog, J., Kiedrzyńska, A. and Badyda, K., "Cfd analysis of natural gas substitution with syngas in the industrial furnaces", ***Energy***, Vol. 179, (2019), 593-602, DOI: 10.1016/j.energy.2019.04.179.
19. Ji, J., Cheng, L., Wei, Y., Wang, J., Gao, X., Fang, M. and Wang, Q., "Predictions of nox/n2o emissions from an ultra-supercritical cfb boiler using a2-d comprehensive cfd combustion model", ***Particuology***, Vol. 49, (2020), 77-87, DOI: 10.1016/j.partic.2019.04.003.
20. Xu, L., Cheng, L., Ji, J., Wang, Q. and Fang, M., "A comprehensive cfd combustion model for supercritical cfb boilers", ***Particuology***, Vol. 43, (2019), 29-37, DOI: 10.1016/j.partic.2017.11.012.
21. Hernik, B., Zabłocki, W., Żelazko, O. and Latacz, G., "Numerical research on the impact of changes in the configuration and the location of the over fire air nozzles on the combustion process in the ultra-supercritical bp 680 boiler", ***Process Safety and Environmental Protection***, Vol. 125, (2019), 129-142, DOI: 10.1016/j.psep.2019.02.029.
22. Modlinski, N. and Hardy, T., "Development of high-temperature corrosion risk monitoring system in pulverized coal boilers based on reducing conditions identification and cfd simulations", ***Applied Energy***, Vol. 204, (2017), 1124-1137, DOI: 10.1016/j.apenergy.2017.04.084.
23. Gómez, M.A., Martín, R., Chapela, S. and Porteiro, J., "Steady cfd combustion modeling for biomass boilers: An application to the study of the exhaust gas recirculation performance", ***Energy Conversion and Management***, Vol. 179, (2019), 91-103, DOI: 10.1016/j.enconman.2018.10.052.
24. Gu, J., Shao, Y. and Zhong, W., "Study on oxy-fuel combustion behaviors in a s-co2 cfb by 3d cfd simulation", ***Chemical Engineering Science***, Vol. 211, (2020), DOI: 10.1016/j.ces.2019.115262.
25. Karim, M.R., Bhuiyan, A.A., Sarhan, A.A.R. and Naser, J., "Cfd simulation of biomass thermal conversion under air/oxy-fuel conditions in a reciprocating grate boiler", ***Renewable Energy***, Vol. 146, (2020), 1416-1428, DOI: 10.1016/j.renene.2019.07.068.
26. Guo, J., Hu, F., Jiang, X., Li, P. and Liu, Z., "Effects of gas and particle radiation on ifrf 2.5 mw swirling flame under oxy-fuel combustion", ***Fuel***, Vol. 263, (2020), DOI: 10.1016/j.fuel.2019.116634.
27. Smith, J.D., Sreedharan, V., Landon, M. and Smith, Z.P., "Advanced design optimization of combustion equipment for biomass combustion", ***Renewable Energy***, Vol. 145, (2020), 1597-1607, DOI: 10.1016/j.renene.2019.07.074.
28. Hu, F., Li, P., Guo, J., Liu, Z., Wang, L., Mi, J., Dally, B. and Zheng, C., "Global reaction mechanisms for mild oxy-combustion of methane", ***Energy***, Vol. 147, (2018), 839-857, DOI: 10.1016/j.energy.2018.01.089.
29. Milcarek, R.J., DeBiase, V.P. and Ahn, J., "Investigation of startup, performance and cycling of a residential furnace integrated with micro-tubular flame-assisted fuel cells for micro-combined heat and power", ***Energy***, Vol. 196, (2020), DOI: 10.1016/j.energy.2020.117148.
30. Si, J., Wang, G., Li, P. and Mi, J., "Optimization of the global reaction mechanism for mild combustion of methane using artificial neural network", ***Energy & Fuels***, Vol. 34, No. 3, (2020), 3805-3815, DOI: 10.1021/acs.energyfuels.9b04413.
31. Hu, C., Luo, K., Zhou, M., Lin, J., Kong, D. and Fan, J., "Influences of secondary gas injection pattern on fluidized bed combustion process: A cfd-dem study", ***Fuel***, Vol. 268, (2020), DOI: 10.1016/j.fuel.2020.117314.
32. Franzelli, B., Riber, E., Gicquel, L.Y.M. and Poinsot, T., "Large eddy simulation of combustion instabilities in a lean partially premixed swirled flame", ***Combustion and Flame***, Vol. 159, No. 2, (2012), 621-637, DOI: 10.1016/j.combustflame.2011.08.004.
33. Garby, R., Selle, L. and Poinsot, T., "Large-eddy simulation of combustion instabilities in a variable-length combustor", ***Comptes Rendus Mécanique***, Vol. 341, No. 1-2, (2013), 220-229, DOI: 10.1016/j.crme.2012.10.020.
34. Fureby, C., "Large eddy simulation of turbulent reacting flows with conjugate heat transfer and radiative heat transfer", ***Proceedings of the Combustion Institute***, (2020), DOI: 10.1016/j.proci.2020.06.285.
35. Shi, Y., Zhong, W., Chen, X., Yu, A.B. and Li, J., "Combustion optimization of ultra supercritical boiler based on artificial intelligence", ***Energy***, Vol. 170, (2019), 804-817, DOI: 10.1016/j.energy.2018.12.172.
36. Paul, C., Haworth, D.C. and Modest, M.F., "A simplified cfd model for spectral radiative heat transfer in high-pressure hydrocarbon–air combustion systems", ***Proceedings of the Combustion Institute***, Vol. 37, No. 4, (2019), 4617-4624, DOI: 10.1016/j.proci.2018.08.024.
37. Perrone, D., Castiglione, T., Klimanek, A., Morrone, P. and Amelio, M., "Numerical simulations on oxy-mild combustion of pulverized coal in an industrial boiler", ***Fuel Processing Technology***, Vol. 181, (2018), 361-374, DOI: 10.1016/j.fuproc.2018.09.001.

Persian Abstract

چکیده

پوشش داخلی محافظ حرارتی دیگ بخار مونواکسید کربن پالایشگاه امام خمینی (ره) شازند چندین بار دچار آسیب شده است، برای ریشه یابی علت این مشکل و تعیین شرایط جدید عملیاتی از دینامیک سالات محاسباتی (CFD) استفاده شد. برای ساده سازی شبیه سازی سه بعدی و کاهش حجم محاسبات از شرط تقارن در شبیه سازی محفظه احتراق استفاده شد، خطوط جریان نشان می‌دهد که استفاده از تقارن خطا در شبیه سازی ایجاد نمی‌کند. تعداد نقاط شبکه بهینه گردید و با استفاده از شرط استقلال نتایج شبیه سازی از تعداد نقاط شبکه، تعداد نقاط شبکه بهینه گردید. شبیه سازی با مکانیسم های احتراق تک مرحله ای، دو مرحله ای، چند مرحله‌ای و مجموع هر سه مکانیسم، انجام گردید و نتایج شبیه سازی با نتایج واقعی اندازه گیری شده از دیگ بخار مونواکسید کربن مقایسه شد، نتایج نشان می دهد که بهترین حالت برای شبیه سازی مجموع مکانیسم‌ها است که خطایی کمتر از 8٪ دارد. پروفایل سرعت و دمای شعله در قسمت های مختلف محفظه احتراق بررسی شد، نتایج نشان می دهد که هرچه از مشعل ها فاصله بگیریم پروفایل سرعت و دما یکنواخت تر می شود همچنین دمای دیواره افزایش پیدا می کند و نحوه اختلاط جریان‌های مختلف ورودی در محفظه احتراق از طریق رسم خطوط جریان بررسی گردید. بررسی پیشرفت واکنش احتراق و مکان یابی مناطق داغ محفظه احتراق و همچنین دمای دیواره ها نتایج نشان می دهد که دمای دیوارمحفظه احتراق در محدوده مناسب است و آسیب حرارتی ندیده است. ولی دیواره مشعل در محل اختلاط جریان ها امکان آسیب جزئی دارد که با تغییر مقدار جریان ها قابل رفع است. پروفایل نامناسب حرارتی همچنین مقدار زیاد اکسیژن در گاز خروجی نشان می دهد که شرایط عملکرد دیگ بخار از شرایط بهینه فاصله دارد و نتایج شبیه سازی نشان می دهد که برای کاهش مقدار CO و NOx در جریان خروجی باید شدت جریان هوای اولیه تغییر کند و همچنین برای جلوگیری از آسیب حرارتی به پوشش داخلی و کاهش خطرات ایمنی، جریان هوای ثانویه تغییر یابد.